Journal of
Applied Crystallography
ISSN 0021-8898
Editor: **Anke R. Pyzalla**

New software for the singular value decomposition of time-resolved crystallographic data

Yi Zhao and Marius Schmidt

J. Appl. Cryst. (2009). **42**, 734–740

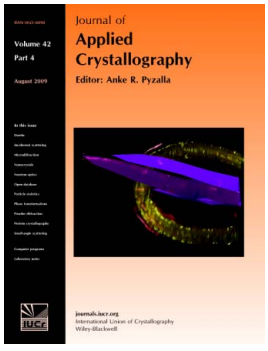

Journal of
Applied Crystallography
ISSN 0021-8898

Received 29 November 2008
Accepted 20 May 2009

New software for the singular value decomposition of time-resolved crystallographic data

Yi Zhao and Marius Schmidt*

Physics Department, University of Wisconsin–Milwaukee, 1900 E. Kenwood Boulevard, Milwaukee, Wisconsin 53211, USA. Correspondence e-mail: m-schmidt@uwm.edu

Singular value decomposition (SVD) has been successfully used in the analysis of time-resolved crystallographic data. A new software package for Linux-based operating systems, called *SVD4TX*, has been developed. In contrast to an earlier version of the SVD program, written in Fortran, the new program provides a GTK+-based graphical user interface for easy user guidance through the entire SVD process. New features, such as an improved, more stable routine to determine a compatible kinetic mechanism, are implemented in the *SVD4TX* program package so that it provides almost all the necessary tools for a semi-automatic and effective SVD-based analysis of time-resolved crystallographic data in one program package.

1. Introduction

Time-resolved crystallography (Moffat, 1989) is a unique technique for determining the structures of intermediates in biomolecular and chemical reactions. It genuinely unifies structure determination with chemical kinetics. A full description of a time-resolved crystallographic experiment would go beyond the scope of this article. The reader is referred to Schmidt (2008) and Schmidt, Ihee *et al.* (2005) for detailed reviews. In short, macromolecular time-resolved crystallography was pioneered in the last two decades of the previous century and came to maturity only recently (Ren *et al.*, 1999). Experiments are of the pump-probe type. A reaction is initiated in a crystal usually by an intense, ultra-short laser flash (the pump) and probed after a time delay Δt by an intense X-ray pulse (the probe) of typically 100 ps duration. Since it is impossible to rotate a crystal substantially during 100 ps, the reflection intensities are collected using still exposures. For this reason, a bandwidth of X-ray radiation is required to collect the integral reflection intensities. Hence, the Laue method is used. The crystal is reoriented to cover the entire reciprocal space (Rajagopal, Kostov & Moffat, 2004). At the end of the experiment, complete data sets of Laue (structure factor) amplitudes at each time delay plus their equivalent reference amplitudes collected from the same crystal in the dark are available. The time delays are preferentially arranged equidistantly in log-time to account for the exponential behavior of chemical kinetics. The data sets are scaled together and time-dependent data sets of weighted difference structure factor amplitudes are obtained (see below). Using phases calculated from a very precise reference structure, difference structure factors are obtained, from which a time-series of difference electron density maps is calculated. The analysis of these four-dimensional data proceeds on the level of difference maps, since difference electron densities and concentrations of the intermediates are linearly dependent on each other (Henderson & Moffat, 1971).

With more and more powerful X-ray sources emerging, time-resolved crystallography will be routinely applied to characterize biologically and pharmaceutically interesting reactions in biomolecules. The simultaneous determination of the structure of reaction intermediates and the kinetics is critical to understanding the mechanism and the pathways by which a protein performs its biological reaction (Schlichting *et al.*, 1990; Bolduc *et al.*, 1995; Ren *et al.*, 2001; Schmidt *et al.*, 2004; Schmidt, Nienhaus *et al.*, 2005; Rajagopal *et al.*, 2005; Ihee *et al.*, 2005; Key *et al.*, 2007; Knapp *et al.*, 2006). Direct structural information on these intermediates is difficult to obtain because they have short lifetimes and tend to overlap heavily in time (Hajdu *et al.*, 2000; Moffat, 2001; Ren *et al.*, 2001; Schlichting, 2003). The other difficulty is the low signal-to-noise ratio of time-resolved crystallographic data, caused by a low fraction of reacting molecules in the crystal. Signal may be difficult to differentiate from noise by simple visual inspection of the electron density maps. For these reasons it was largely unknown how to extract the structure information and separate it from the kinetics (Moffat, 2001). This problem was solved by applying singular value decomposition (SVD; Golub & Reinsch, 1970), a powerful technique for dealing with sets of equations or matrices, to crystallographic data (Schmidt *et al.*, 2003). SVD may act as a noise filter, and it determines the main components found in a time-resolved crystallographic experiment.

SVD is a widely used technique (Henry & Hofrichter, 1992) for decomposing a matrix into several component matrices, exposing many of the useful and interesting properties of the original matrix (see also Hansen *et al.*, 2006). The SVD method is based on the following theorem of linear algebra: Any $m \times n$ matrix $\mathbf{A}$ whose number of rows m is greater than or equal to its number of columns n can be written as the product of an $m \times n$ column-orthogonal matrix $\mathbf{U}$, an $n \times n$ diagonal matrix $\mathbf{S}$ with positive or zero elements (the singular values), and the transpose of an $n \times n$ orthogonal matrix $\mathbf{V}$:

$$\mathbf{A} = \mathbf{U}\mathbf{S}\mathbf{V}^{\mathrm{T}}. \quad (1)$$

The columns of $\mathbf{U}$ and $\mathbf{V}$ are called the left singular vectors and right singular vectors of $\mathbf{A}$, respectively. The diagonal elements of $\mathbf{S}$ are called the singular values of $\mathbf{A}$.

In the analysis of time-resolved X-ray data, the SVD method separates time and space variables. From a series of time-dependent difference maps it determines only a few main common spatial components and their time variations, which constitute main common temporal components. The temporal components are then used to determine the number of intermediate states and relaxation times.

The relaxation times of the kinetics can be faithfully found in a global way in the right singular vectors. These relaxation times may be used to estimate a kinetic mechanism which can be fitted to the data. From such a fit, the pure difference electron density maps of the intermediates can be determined. Finally, the structures of the intermediates are modeled with the help of these difference maps.

The applicability of SVD to crystallographic data was initially demonstrated by Schmidt *et al.* (2003) using mock data. The SVD method was applied to calculated difference Fourier maps, simulating those to be obtained in a time-resolved crystallographic study of photoactive yellow protein. Random noise of varying levels in the difference structure factor amplitudes, different extents of reaction initiation and different numbers of time points were all employed to simulate a range of realistic experimental conditions. The results showed that SVD allows for an unbiased differentiation between signal and noise, which laid the basis for a noise reduction procedure called SVD flattening; this ultimately led to noise-reduced and phased difference maps. These maps can be used to further identify and fit a kinetic mechanism, a prerequisite for extracting the difference electron densities and the structures of the intermediates. The SVD-based procedures were then used in multiple studies to analyze real time-resolved crystallographic data (Rajagopal, Schmidt *et al.*, 2004; Rajagopal *et al.*, 2005; Schmidt *et al.*, 2004; Schmidt, Nienhaus *et al.*, 2005; Schmidt, Ihee *et al.*, 2005; Ihee *et al.*, 2005; Key *et al.*, 2007). For the SVD analysis of time-resolved X-ray data a number of programs needed to be used; the central program was called *SVD4TX* ('singular value decomposition for time-resolved X-ray data'; Schmidt *et al.*, 2003). *SVD4TX* was written in Fortran and implemented the SVD algorithm and most procedures necessary for the kinetic analysis of the time-resolved crystallographic data. However, additional, stand-alone programs were used to perform basic operations such as calculation of weighted difference structure factors, Fourier transforms, quality factor analysis (Rajagopal, Schmidt *et al.*, 2004) and phase recombination in SVD flattening. In addition, new routines had to be programmed and linked to *SVD4TX* for each candidate chemical kinetic mechanism to be tested; hence, substantial effort and expert knowledge was needed to perform an SVD analysis of crystallographic data.

Although *SVD4TX* can be used with any crystallographic data that depend on an additional parameter such as pH, temperature or dose, the program was mainly developed having time-resolved macromolecular crystallographic data in mind. Based on the existing program in Fortran, a new *SVD4TX* program package with a graphical user interface is described in this paper. The goals of the new program are to create a computational framework for the SVD analysis and to provide all necessary tools for the SVD analysis of time-resolved crystallographic data in one program package. Compared with the Fortran version, some new features, such as an efficient fast Fourier transform (FFT) routine, SVD flattening, quality factor analysis and a general routine to diagonalize coefficient matrices, were newly implemented; the fit routines were also improved and are more stable. Altogether, this amounts to a flexible, easy to use program for anyone who wishes to analyze crystallographic data by the singular value decomposition method. To demonstrate the ability of the new *SVD4TX*, we have used time series of mock data generated by the method described by Schmidt *et al.* (2003) with experimental noise included to simulate the experimental conditions as closely as possible.

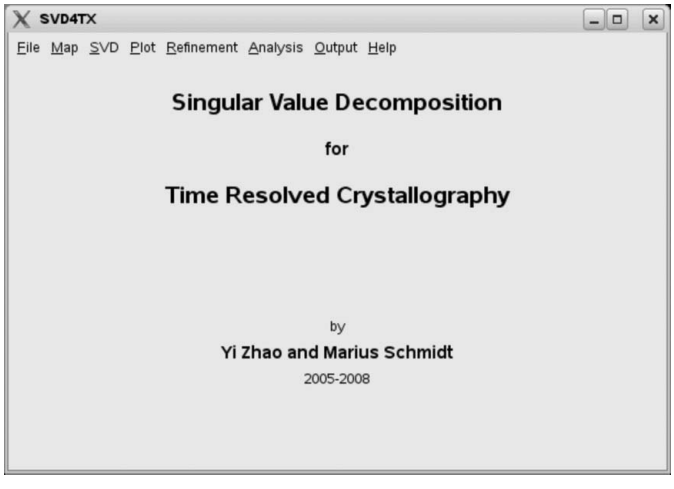

Figure 1
The interface of the software package *SVD4TX* which appears when the program is started.

2. Description of the new *SVD4TX* program package

The source code of the *SVD4TX* program is written in C for Linux-based operating systems. This new program package provides a GTK+ 2.0-based graphical user interface for easy user guidance. Fig. 1 shows the interface of *SVD4TX*. The goals of the SVD analysis are the determination of a chemical kinetic mechanism and the extraction of pure difference electron densities of the intermediates from the crystallographic data. The procedures to reach those goals are schematically shown in Fig. 2. In short, there are four major steps involved in the processing of the data: Step 1 involves the Fourier transformation of time-dependent structure factors to difference electron densities, from which the data matrix is constructed. The time information is then used in step 2 to reduce the noise in the difference maps by means of SVD flattening. In step 3, a number of exponentials are fitted to determine relaxation times in a global way. A candidate chemical kinetic mechanism is then selected in step 4 to extract the difference electron densities of the intermediates.

2.1. Format of input data

SVD4TX analyzes a time series of crystallographic data. In order to simplify the input process, an input file in text format must be prepared (Fig. 3), which is read by the program. Two types of data formats are now supported by the program: structure factors and difference electron density maps. At present, the FSFOUR map

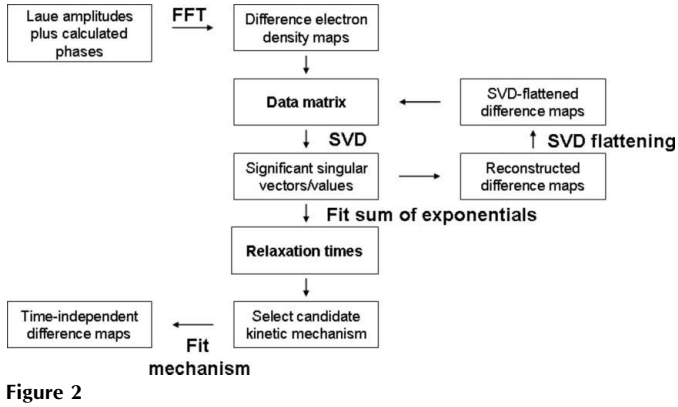

Figure 2
The procedures of *SVD4TX*. Four major steps are involved in the processing of the data to finally generate the time-independent difference maps of the intermediates: preparation of data, SVD and SVD flattening, fit of a sum of exponentials, and determination of a chemical kinetic mechanism.

format is supported for compatibility with the *XtalView*/*Xfit* molecular graphics suite (McRee, 1999). The location of time-dependent structure factor amplitude data and those of the corresponding initial (dark) state must be included in the input file.

The input file in Fig. 3 shows a typical time series that would be obtained from a time-resolved experiment. Four crystals were used to generate the time series from 1 µs to 100 ms. Five time-dependent data sets, $|\mathbf{F}(hkl, t)|$, plus one reference data set (in the dark, $|\mathbf{F}^{\rm D}(hkl)|$) were measured per crystal. Each data set consists of a list of h, k, l Laue structure factor amplitudes plus their uncertainties (σ). The reference data sets (ref1.hkl to ref4.hkl in this example) need to be scaled beforehand to a data set calculated from a precise initial (dark) state model. This brings them to the absolute scale. The time-dependent data sets should be scaled to their respective reference data. As a result, all data are on the absolute scale.

The file containing the calculated structure factors of the initial (dark) state including the phase has to be supplied (2phy_fc6.phs in Fig. 2). An atomic model used for mask building purposes is read in PDB file format (Protein Data Bank; Berman *et al.*, 2000). In addition, the symmetry operators must be supplied. The program searches the keywords (see Fig. 3) to assign file paths and parameters. Difference maps can be used instead of structure factors. In this case, the location of the difference maps should be included following the keyword 'MAP FILES'.

2.2. From structure factors to electron density

With the implemented FFT routine (Singeleton, 1968), the time-dependent difference electron density maps are calculated from the set of time-dependent structure factor amplitudes $|\mathbf{F}(hkl, t)|$, the corresponding structure factor amplitudes of the initial (dark) state $|\mathbf{F}^{\rm D}(hkl)|$ and the phases $\varphi^{\rm C}$ calculated from the known reference atomic model. The difference electron densities are calculated as

$$\Delta\rho(t) = \frac{1}{V_{\rm e}} \sum_{hkl} w \Delta F(hkl, t) \exp(i\varphi^{\rm C}_{hkl}) \exp[-2\pi i(hx + ky + lz)], \quad (2)$$

where x, y, z are the components of the position vector in the coordinate system of the unit cell (fractional coordinates), h, k, l are the reflection indices, $V_{\rm e}$ is the volume of the unit cell and w is a weighting factor for the difference structure factor amplitude $\Delta F(hkl, t)$. The weighting of difference electron densities reduces the influence of outliers and inaccurately determined reflection intensities. The weighting factor is calculated according to Ren *et al.* (2001) as

$$w = \frac{1}{1 + \Delta F^2/\langle \Delta F^2 \rangle + \sigma^2_{\Delta F}/\langle \sigma^2_{\Delta F} \rangle}, \quad (3)$$

where $\sigma_{\Delta F}$ is the variance of ΔF, and $\langle \Delta F^2 \rangle$ and $\langle \sigma^2_{\Delta F} \rangle$ are the mean values of ΔF^2 and $\sigma^2_{\Delta F}$. For the calculation of electron density maps a few parameters such as the resolution limit, the grid numbers and the direction of the plane should be given in a dialog window (Fig. 4). To refine this process, *SVD4TX* divides the data into a few resolution shells (typically 5–10) and the weighting factors are calculated in the individual resolution shell. In this case, $\langle F^2 \rangle$ and $\langle \sigma^2_{\Delta F} \rangle$ are the mean values of ΔF^2 and $\sigma^2_{\Delta F}$ in the individual resolution shells. The maximum resolution found in the data is suggested as the resolution limit in the dialog window, which can be changed manually. The suggested grid numbers can also be changed manually. The difference maps are then saved in FSFOUR format.

The structure factor amplitudes and phases will also be used later for the newly implemented procedure of SVD flattening. If, similar to the former version of *SVD4TX*, already existing time-dependent difference maps are imported to the program, the process of FFT may be omitted. This option is useful for a quick check. However, then, SVD flattening is not possible since it needs structure factors and σ values for phase recombination. It is, therefore, strongly recommended that the time-dependent Laue amplitudes with calculated phases are used for the entire SVD analysis.

2.3. Singular value decomposition

The SVD procedure separates time and space variables. The left singular vectors are difference maps; they are the main spatial components of the experimental, time-dependent difference maps. Each right singular vector contains the temporal variation of the corresponding left singular map, whereas the singular values weight

```
PDBFILE  2ms.pdb                                  pdb-file for mask
SYMMETRY OPERATORS 6                              symmetry operators
X,Y,Z
-Y,X-Y,Z
Y-X,-X,Z
-X,-Y,1/2+Z
Y,Y-X,1/2+Z                                       read in: structure factors amplitudes
X-Y,X,1/2+Z                                       write out: difference maps in FSFOUR format
PHASE FILES FSFOUR 21
1.0E-6    DATA/tp1.hkl   ref1.hkl  1.00          time points
1.8E-6    DATA/tp2.hkl   ref2.hkl  1.05          column 1: time
3.2E-6    DATA/tp3.hkl   ref3.hkl  1.02          column 2: time-dependent Laue-amplitudes
5.6E-6    DATA/tp4.hkl   ref4.hkl  1.08          column 3: reference (dark ) data for this
10.0E-6   DATA/tp5.hkl   ref1.hkl  1.00                    particular crystal
18.0E-6   DATA/tp6.hkl   ref2.hkl  1.05          column 4: normalizing factor to correct
32.0E-6   DATA/tp7.hkl   ref3.hkl  1.02                    for variations in reaction initiation
56.0E-6   DATA/tp8.hkl   ref4.hkl  1.08                    (Laser power)
100.0E-6  DATA/tp9.hkl   ref1.hkl  1.00
180.0E-6  DATA/tp10.hkl  ref2.hkl  1.05
320.0E-6  DATA/tp11.hkl  ref3.hkl  1.02
560.0E-6  DATA/tp12.hkl  ref4.hkl  1.08
1.0E-3    DATA/tp13.hkl  ref1.hkl  1.00
1.8E-3    DATA/tp14.hkl  ref2.hkl  1.05
3.2E-3    DATA/tp15.hkl  ref3.hkl  1.02
5.6E-3    DATA/tp16.hkl  ref4.hkl  1.08
10.0E-3   DATA/tp17.hkl  ref1.hkl  1.00
18.0E-3   DATA/tp18.hkl  ref2.hkl  1.05
32.0E-3   DATA/tp19.hkl  ref3.hkl  1.02
56.0E-3   DATA/tp20.hkl  ref4.hkl  1.08
100.0E-3  DATA/tp21.hkl  ref1.hkl  1.00          calculated structure factors
DARK_CALC 2phy_fc6.phs                            from precise reference model
```

Figure 3
An example of an input file. The keywords are described. The file paths of the structure factor data (or difference maps for a quick check), a PDB file to calculate a mask and the symmetry operators are needed.

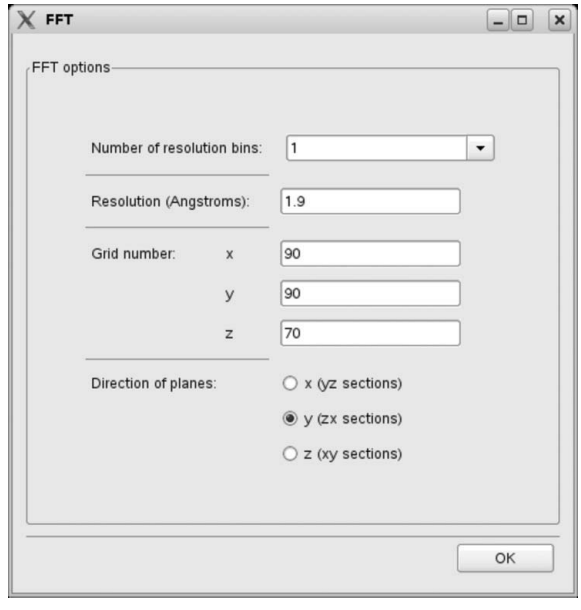

Figure 4
Dialog for FFT options. The maximum resolution found in the data is suggested as resolution limit, which can be manually changed. The suggested number of grid points is based on Shannon sampling (Fung *et al.*, 2009), implying voxels with edge lengths roughly half the maximum resolution limit.

the contribution of the components to the experimental difference maps.

To perform an SVD analysis, data matrix **A** is prepared, where the difference maps from a time series are entered one by one and in temporal order as column vectors of the matrix. Since a unit cell in macromolecular crystallography can easily consist of half a million grid points, the number of grid points should be reduced to make the calculation faster. If crystallographic symmetry is present, only the asymmetric unit needs to be included. What is more, a mask can be calculated by the program using the PDB file to include only the volume occupied by protein atoms. A further reduction in the number of considered grid points is possible if those that do not contain significant difference electron densities throughout the time course are disregarded. For this purpose, the program allows the option of selecting grid points only if the positive difference electron density is above, or the negative difference electron density is below, a chosen σ level for at least one time point; thus, the number of useful grid points can be reduced to around 10^4–10^5 for moderately sized unit cells.

The *SVD4TX* package provides a dialog window in which one can determine SVD options such as an additional margin to the mask and select the σ level to prepare matrix **A**, which will then decompose to the left and right singular vectors and the singular values.

Not all of the singular vectors contain signal. The number of significant singular vectors is related to the number of intermediates in the reaction (Henry & Hofrichter, 1992; Schmidt, Ihee *et al.*, 2005; Schmidt, 2008). However, the structure information available to crystallography adds powerful methods to further guide this discrimination. First, the left singular vectors are difference maps and can be displayed on a graphics screen together with suitable atomic models, for example, that of the reference state. Signal is faithfully detected (Schmidt *et al.*, 2003). Secondly, the difference electron density in regions of large signal can be used to automatically determine a quality factor (Rajagopal, Schmidt *et al.*, 2004; see below), and the discrimination can be based on this. In addition, the autocorrelation of the right singular vectors can be employed for an estimate. The method of rotation (Henry & Hofrichter, 1992; Schmidt *et al.*, 2003) is implemented in the new *SVD4TX* to re-collect the signal from the less significant singular vectors into the more significant. Nevertheless, whichever method is used, a set of significant singular values and vectors is the result. As an example, Fig. 5 shows a set of significant right singular vectors.

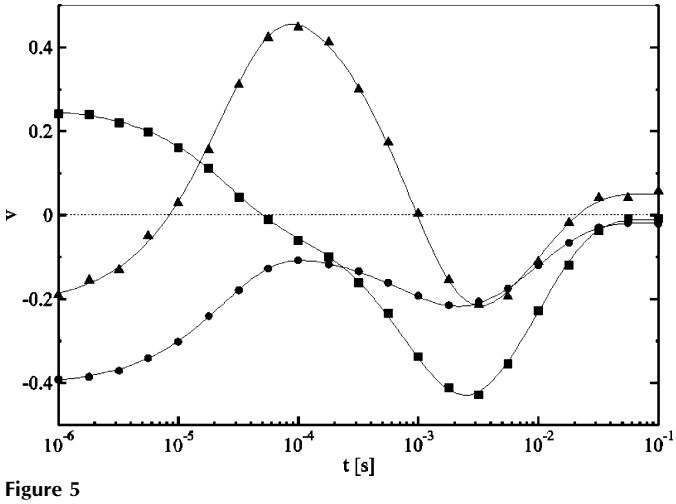

Figure 5
Right singular vectors from the SVD analysis. Their amplitudes are weighted by the square of their corresponding singular value. The first three (significant) right singular vectors are shown in the figure with solid spheres, squares and triangles, respectively. The fitted exponential curves are shown as solid lines.

Using only significant singular values and vectors to reconstruct the data matrix **A** and ignoring the insignificant singular vectors containing only noise and no signal, the signal-to-noise ratio in the reconstructed difference maps is improved. The data matrix **A** can then be approximated in a least-squares sense by matrix **A**′:

$$\mathbf{U}'\mathbf{S}'\mathbf{V}'^{\mathrm{T}} = \mathbf{A}' \simeq \mathbf{A}. \tag{4}$$

This new, noise-reduced data matrix **A**′ constitutes the basis for the SVD flattening.

2.4. SVD flattening

SVD flattening (Schmidt *et al.*, 2004; Schmidt, Ihee *et al.*, 2005; Schmidt, 2008), a new procedure to use time information for noise reduction, is now implemented in the *SVD4TX* program package. From the noise-reduced difference maps, which are reconstructed with only the significant singular values and vectors, difference structure factors with amplitude $\Delta\mathbf{F}_t^{\mathrm{SVD}'}$ and phase $\varphi_{\Delta F}^{SVD'}$ are obtained by an inverse Fourier transform. These structure factors are combined with the structure factors of the dark state by a phase recombination scheme to obtain improved structure factors. The procedure of phase recombination is shown schematically in Fig. 6. First, we divide the data into a small number of resolution shells, each of which contains roughly the same number of data. The following procedure is performed for each resolution shell. The phase of time-dependent, measured Laue amplitudes, φ_{Ft}, is approximately equal to the phase of the vector sum of $\Delta\mathbf{F}_t^{\mathrm{SVD}'}$ and the calculated structure factor of the dark state $\mathbf{F}_{\mathrm{C}}$ (see Fig. 6). The amplitude of the calculated structure factor $\mathbf{F}_{\mathrm{C}}$ is usually not equal to that measured from the crystal in the dark, $\mathbf{F}_{\mathrm{O}}$, because of crystal-to-crystal differences. To correct for this and to allow for the information of the precise reference (dark state) model to enter the analysis, we calculated

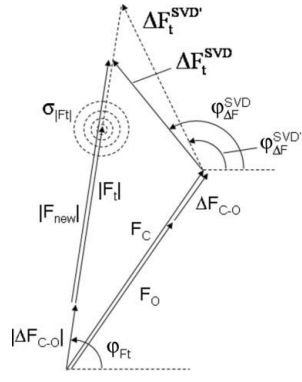

Figure 6
Argand diagram for phase recombination in SVD flattening. $\mathbf{F}_{\mathrm{C}}$: reference structure factor (amplitude and phase) calculated from a precise reference (dark state) model. $\mathbf{F}_{\mathrm{O}}$: observed reference (dark) structure factor amplitude having the same phase as $\mathbf{F}_{\mathrm{C}}$. $\Delta\mathbf{F}_{\mathrm{C-O}}$: difference between structure factor amplitude measured as a reference and that calculated from the reference model; allows to correct for crystal-to-crystal differences and to include information from the precise dark state model. $\Delta\mathbf{F}_t^{\mathrm{SVD}'}$, $\varphi_{\Delta F}^{\mathrm{SVD}'}$: difference structure factor amplitude and phase obtained by Fourier inversion of the noise-reduced time-dependent difference map reconstructed by using only the most significant singular values and vectors. $|\mathbf{F}_t|$: measured time-dependent (Laue) structure factor amplitude; its direction (phase) is given by $\mathbf{F}_{\mathrm{C}} + \Delta\mathbf{F}_t^{\mathrm{SVD}'}$; $|\Delta\mathbf{F}_{\mathrm{C-O}}|$ is added to $|\mathbf{F}_t|$ to bring it to the scale of the calculated reference structure factors. $\sigma_{|Ft|}$: uncertainty (noise) of $|\mathbf{F}_t|$ determined by the data reduction software. If the noise is small relative to the overall noise, $\Delta\mathbf{F}^{\mathrm{SVD}}$ with phase $\varphi_{\Delta F}^{\mathrm{SVD}}$ will point to the tip of $|\mathbf{F}_t|$; otherwise it will point to the tip of $\Delta\mathbf{F}_t^{\mathrm{SVD}'}$. Here, an intermediate situation is pictured. New, noise-improved difference electron density maps are calculated from $\Delta\mathbf{F}^{\mathrm{SVD}}$.

Table 1
Quality factors from the left singular vectors from a time series of 21 time-dependent mock data sets.

Two different spatial positions were evaluated for quality factor 1 and quality factor 2.

Left singular vectors	Quality factor 1	Quality factor 2
1	2.57	2.13
2	1.82	1.47
3	2.99	1.43
4	1.38	0.93
5	0.87	0.79
6	0.97	0.66
7	0.83	0.77
8	1.36	1.09
9	1.21	0.69
10	1.10	0.69
11	0.81	0.78
12	0.98	0.87
13	1.17	0.89
14	1.16	0.62
15	0.89	0.72
16	0.84	0.82
17	1.14	1.06
18	1.01	0.95
19	1.00	0.93
20	0.83	0.75
21	1.30	0.64

$|\Delta\mathbf{F}_{C-O}|$ by subtracting the observed dark state Laue amplitude $|\mathbf{F}_O|$ from $|\mathbf{F}_C|$. The addition of $|\Delta\mathbf{F}_{C-O}|$ to $|\mathbf{F}_t|$ corrects for differences that influence both the dark state Laue amplitudes and the time-dependent Laue amplitudes. The amplitude of an improved structure factor $|\mathbf{F}_{new}|$ is calculated (see below), which takes into account the relative noise, which is the uncertainty of $|\mathbf{F}_t|$, σ_{Ft}, relative to the mean uncertainty found in that resolution shell, $\langle\sigma_{Ft}\rangle$. For this a weighting factor p_{res} is calculated, which accounts for the relative noise:

$$p_{res} = \frac{1}{1 + \sigma_{Ft}^2/\langle\sigma_{Ft}^2\rangle_{res}}. \quad (5)$$

p_{res} is then used to calculate the amplitude $|\mathbf{F}_{new}|$:

$$|\mathbf{F}_{new}| = p_{res}(|\mathbf{F}_t| + |\Delta\mathbf{F}_{C-O}|) + (1 - p_{res})|\mathbf{F}_C + \Delta\mathbf{F}_t^{SVD}|. \quad (6)$$

In the case of low relative noise, $|\mathbf{F}_{new}|$ will be $|\mathbf{F}_t| + |\Delta\mathbf{F}_{C-O}|$. If the relative noise is very large, then $|\mathbf{F}_{new}|$ will be $|\mathbf{F}_C + \Delta\mathbf{F}_t^{SVD}|$. In Fig. 6 an intermediate situation is sketched, which results in improved difference structure factors $\Delta\mathbf{F}_t^{SVD}$ (amplitude and phase). New difference electron density maps with improved signal-to-noise ratio are then obtained by Fourier transforming these $\Delta\mathbf{F}_t^{SVD}$. The improvement of the phases of the SVD-flattened structure factors is of the order of 10–15° depending on the noise level (Schmidt *et al.*, 2003). The SVD-flattened difference maps can then be subjected to SVD flattening again until convergence is reached. These maps are much better suited for interpretation and further analysis. Fig. 7 shows a difference map of a single time point before and after SVD flattening.

2.5. Quality factor analysis

The quality factor analysis is a new feature of the program *SVD4TX*. It can be used to estimate the signal-to-noise ratio of individual difference maps, and it has been applied to analyze experimental time-resolved crystallographic data by Rajagopal and co-workers (Rajagopal, Schmidt *et al.*, 2004; Rajagopal *et al.*, 2005) and by Ihee *et al.* (2005). The quality factor is evaluated using left singular vectors, which are difference maps. The quality factor is defined here as the ratio of the mean absolute difference electron density in a spherical region of diameter of 2–3 Å within a signal region to the σ value of the whole map. *SVD4TX* looks for two regions with the largest signals separated by at least 5 Å, integrates the absolute difference electron densities in the mentioned spherical region and calculates quality factors. A larger quality factor means more significant signal in the map. Only maps with the highest quality factors are significant and will be selected for further analysis. The quality factor analysis allows for an unbiased, automatic approach to evaluating the significance of the left singular vectors. An example of the calculated quality factors of left singular vectors is shown in Table 1. It is obvious from these values that the first three left singular vectors have significantly high quality factors and therefore high signal-to-noise ratio. In combination with the other criteria mentioned above and below, one can faithfully determine that for our example here the first three singular vectors and values are significant, and it is with these that the analysis proceeds.

2.6. Kinetic mechanisms from the SVD

SVD4TX can fit kinetic mechanisms consisting of first-order reactions to the data. As mentioned above, the right singular vectors show the temporal variation of the corresponding left singular vectors. The time courses in the right singular vectors are linear combinations of the time-dependent concentrations of intermediates. For first-order reactions, the concentrations obey exponential functions (Steinfeld *et al.*, 1989). Therefore, the relaxation times τ_j of these reactions can be determined by globally fitting a sum of exponential terms featuring common relaxation times to the significant right singular vectors:

$$v_n(t) = \sum_{j=1}^{J} A_{n,j} \exp(-t/\tau_j), \quad (7)$$

where v_n is the nth significant right singular vector and J is the number of exponential functions found globally (Fig. 5). The pre-exponentials $A_{n,j}$ and the relaxation times τ_j are the fit parameters.

In the program package *SVD4TX*, a more stable fit routine that minimizes the sum of the squares of m nonlinear functions in n variables by a modification of the Levenberg–Marquardt algorithm (Garbow *et al.*, 1980) is employed. Initial values of relaxation times can be roughly estimated from the plot of right singular vectors and

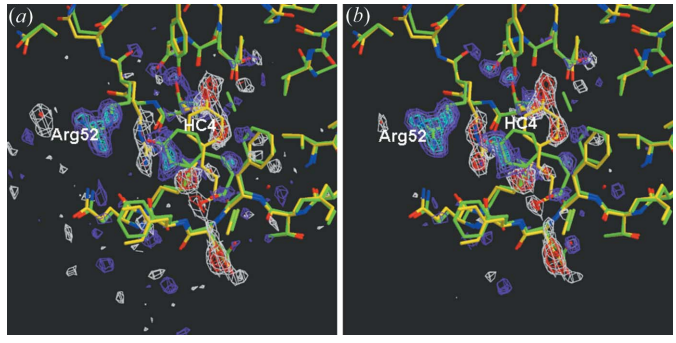

Figure 7
Difference maps of a single time point (time point 15, 3.2 ms) before (*a*) and after (*b*) SVD flattening using the time course of 21 time-dependent mock data sets. The noise in the mock data is roughly equivalent to four times the experimental noise [see Schmidt *et al.* (2003) for a description of how to add noise to mock data]. The improvement of the signal-to-noise ratio in the difference electron density is apparent. Red and white: negative difference electron density on the $-3\sigma/-4\sigma$ level; blue and cyan: positive difference electron density on the $3\sigma/5\sigma$ level, respectively. The atomic models of the reference dark state (in yellow) and the third intermediate (in green) are overlaid to guide the eye. HC4 and Arg52: hydroxycinnamic acid and arginine 52 moieties were used to simulate prominent structural changes.

are input manually in a dialog window. The program finds the best fitted values of relaxation times and the corresponding amplitudes of the exponentials. In the example in Fig. 5 the three relaxation times are found to be 30 µs, 800 µs and 10 ms.

In order to fit a kinetic mechanism, the number of intermediates involved has to be estimated from the data. As mentioned earlier, the numbers of significant singular values and vectors are related to the number of intermediates. However, because of noise in the data, part of the signal may cross-talk into less significant singular vectors and values (Schmidt *et al.*, 2003), which makes an estimate difficult. On the other hand, the relaxation times are also related to a possible chemical kinetic mechanism in a very specific way. In general, the number of relaxation times is equal to the number of intermediates plus the initial (dark) state (Matsen & Franklin, 1950; Fleck, 1971; Steinfeld *et al.*, 1989). Since the relaxation times can be accurately determined from the global analysis described above, the number of intermediates can be faithfully determined from them. If J relaxation times are determined in the previous step, the program offers a dialog window to select a candidate mechanism by checking the boxes with the corresponding rate coefficients k from a general mechanism that employs the J states, plus the initial (dark) state, as shown in Fig. 8. For the selected candidate mechanism, the program suggests the initial values of rate coefficients k; no expert user knowledge will be required. With the selected candidate mechanism, a coefficient matrix of the rate coefficients is formed. By diagonalizing the coefficient matrix eigenvalues are obtained (Peters & Wilkinson, 1971), which are in turn the relaxation times τ_j present in the exponential functions [equation (7)]. By varying the rate coefficients k in the coefficient matrix, and therefore the eigenvalues of the coefficient matrix, the program determines the best fitting rate coefficients. Once the rate coefficients are obtained, the concentration profiles for each intermediate j, $I_j(k, t)$ ($j = 1, \ldots, J$), for the selected candidate mechanism can be calculated. As examples, the sequential mechanism and dead end mechanism are selected. These mechanisms each employ three intermediates, I_1, I_2 and I_3, plus the initial state, I_0. The fitted rate coefficients are $k(I_1 \rightarrow I_2) = 35000\ \mathrm{s}^{-1}$, $k(I_2 \rightarrow I_3) = 1200\ \mathrm{s}^{-1}$, $k(I_3 \rightarrow I_0) = 75\ \mathrm{s}^{-1}$ for the sequential mechanism and $k(I_1 \rightarrow I_2) = 35000\ \mathrm{s}^{-1}$, $k(I_2 \rightarrow I_3) = 700\ \mathrm{s}^{-1}$, $k(I_3 \rightarrow I_2) = 350\ \mathrm{s}^{-1}$, $k(I_2 \rightarrow I_0) = 280\ \mathrm{s}^{-1}$ for the dead end mechanism, respectively. From this, the concentrations of the intermediates are calculated. They are shown in Fig. 9. It should be mentioned at this point that multiple mechanisms can fit the data equally well (Schmidt *et al.*, 2004). Especially for more complex kinetic schemes, additional information obtained, for example, from time-resolved spectroscopy (De la Mora-Rey & Wilmot, 2007) may be required to distinguish between the degenerated mechanisms. Although all intermediates that populate significantly can be extracted from the crystallographic data, a unique kinetic mechanism is needed to finally decide whether these intermediates are on or off the catalytic path.

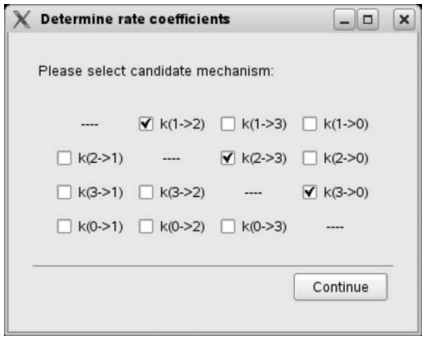

Figure 8
Example for the selection of a candidate mechanism from a reaction employing three intermediates plus the initial (dark) state. The rate coefficients are those that would appear in a coefficient matrix describing this reaction after instantaneous initiation. Here a sequential mechanism is selected by checking the boxes with the corresponding rate coefficients.

2.7. Calculation of time-independent electron density data of intermediates

During the fit of the concentrations of intermediates to the right singular vectors, the linear scale factors $E_{n,j}$ were determined:

$$s_n^2 v(t)_n^{\mathrm{obs}} \simeq v(t)_n^{\mathrm{fit}} = s_n^2 \sum_j E_{n,j} I_j(k, t), \qquad (8)$$

where $v(t)_n^{\mathrm{obs}}$ and $v(t)_n^{\mathrm{fit}}$ are the nth observed and fitted right singular vectors, respectively. The fit is weighted by the square of the corresponding singular value s_n^2. The scale factor $E_{n,j}$ determines the

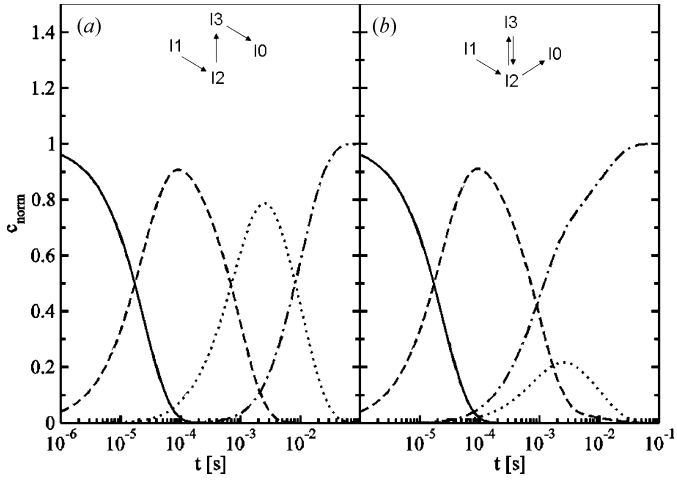

Figure 9
Fractional concentrations of intermediates (c_{norm}) for the simplified mechanisms as a function of time t: sequential (*a*) and dead end (*b*) mechanisms employing three intermediates, I_1, I_2 and I_3, plus the initial (dark) state, I_0. Solid, dashed and dotted lines: time-dependent concentrations of I_1, I_2 and I_3, respectively. Dashed–dotted line: concentration of the reference state I_0.

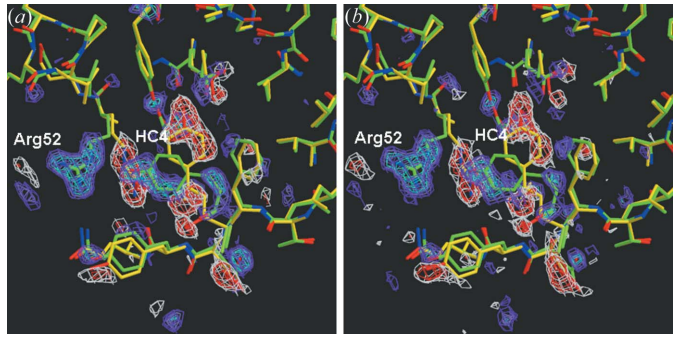

Figure 10
The time-independent difference electron density of the third intermediate. (*a*) Original, noise- and error-free, phased difference electron density of intermediate 3. This intermediate was used together with two other intermediates to calculate the time-dependent mock data. (*b*) Time-independent difference map of intermediate 3, which has been extracted from the time course of mock data containing about four times the experimental noise. Red and white: negative difference electron density on the $-3\sigma/-4\sigma$ level; blue and cyan: positive difference electron density on the $3\sigma/5\sigma$ level, respectively. The atomic model of this intermediate (in green) as well as that of the reference dark state (in yellow) is overlaid to guide the eye. HC4 and Arg52: hydroxycinnamic acid and arginine 52 moieties were used to simulate prominent structural changes.

contribution of the nth left singular vector to the difference map of the jth intermediate. The $E_{n,j}$ parameters can be used to calculate the pure, time-independent difference electron density, $\Delta\rho_{I,j}$, of the jth ($j = 1, \ldots, J$) intermediate employed by the mechanism using only the significant left singular vectors and the significant singular values (Henry & Hofrichter, 1992; Schmidt *et al.*, 2003). In other words, the $E_{n,j}$ values project the left singular vectors u_n onto the intermediate states:

$$\Delta\rho_{I,j} = \sum_n u_n s_n E_{n,j}. \quad (9)$$

This is equivalent to separating the mixture of intermediates from the time-dependent difference maps. These, now time-independent, difference maps constitute the final result of the SVD analysis (see Fig. 10 as an example) and can be used to compute the extrapolated conventional electron density maps in which the atomic structures of the intermediates are modeled (Genick *et al.*, 1997; Schmidt *et al.*, 2004; Ihee *et al.*, 2005; Rajagopal *et al.*, 2005).

3. Conclusion

The software package *SVD4TX* with graphical user interface was developed to perform an analysis of time-resolved crystallographic data based on singular value decomposition almost instantly in a user friendly way. The new *SVD4TX* covers almost all the necessary tools for SVD analysis of time-resolved crystallographic data. One of the new features of *SVD4TX* is that the time-dependent difference electron density maps can be calculated from a set of time-dependent structure factor amplitudes obtained from a time-resolved crystallographic experiment, a corresponding data set of reference amplitudes and phases obtained from the known dark state atomic model. Quality factor analysis provides the possibility to select the most significant left singular vectors by estimating the signal-to-noise ratio of individual maps. A sophisticated SVD-flattening procedure is available within the same software package. A general approach to solve a series of differential equations to calculate the concentrations of the intermediates is implemented. This approach diagonalizes the coefficient matrix that describes a kinetic mechanism of first-order reactions. A fit to the data that uses this approach is more stable and yields faithful results. The structured design of the program allows for easy implementation of the new features of this program and of the new kinetic mechanism with an arbitrarily large number of intermediates.

This work was supported in part by the College of Letters and Sciences of the University of Wisconsin–Milwaukee, USA, and by the Deutsche Forschungsgemeinschaft, SFB 533 and grant Schm 1423/2-1.

References

Berman, H. M., Westbrook, J., Feng, Z., Gilliland, G., Bhat, T. N., Weissig, H., Shindyalov, I. N. & Bourne, P. E. (2000). *Nucleic Acid Res.* **28**, 235–242.
Bolduc, J. M., Dyer, D. H., Scott, W. G., Singer, P., Sweet, R. M., Koshland, D. E. & Stoddard, B. L. (1995) *Science*, **268**, 1312–1318.
De la Mora-Rey, T. & Wilmot, C. M. (2007). *Curr. Opin. Struct. Biol.* **17**, 580–586.
Fleck, G. M. (1971). *Chemical Reaction Mechanism*. New York: Holt, Rinehart and Winston.
Fung, R., Shneerson, V., Saldin, D. K. & Ourmazd A. (2009). *Nat. Phys.* **5**, 64–67.
Garbow, B. S., Hillstrom, K. E. & More, J. J. (1980). *MINPACK Project*. Argonne National Laboratory, Illinois, USA.
Genick, U. K., Borgstahl, G. E., Ng, K., Ren, Z., Pradervand, C., Burke, P. M., Srajer, V., Teng, T. Y., Schildkamp, W., McRee, D. E., Moffat, K. & Getzoff, D. E. (1997). *Science*, **275**, 1471–1475.
Golub, G. H. & Reinsch, C. (1970). *Numer. Math.* **14**, 402–420.
Hajdu, J., Neutze, R., Sjögren, T., Edman, K., Szöke, A., Wilmouth, R. C. & Wilmot, C. M. (2000). *Nat. Struct. Biol.* **7**, 1006–1012.
Hansen, P. C., Nagy, J. G. & O'Leary, D. P. (2006). *Deblurring Images: Matrices, Spectra, and Filtering*, Siam Series on Fundamentals of Algorithms. Philadelphia: Society for Industrial and Applied Mathematics.
Henderson, R. & Moffat, J. K. (1971). *Acta Cryst.* B**27**, 1414–1420.
Henry, E. R. & Hofrichter, J. (1992). *Methods Enzymol.* **210**, 129–192.
Ihee, H., Rajagopal, S., Srajer, V., Pahl, R., Schmidt, M., Schotte, F., Anfinrud, P. A., Wulff, M. & Moffat, K. (2005). *Proc. Natl Acad. Sci. USA*, **102**, 7145–7150.
Key, J., Srajer, V., Pahl, R. & Moffat, K. (2007). *Biochemistry*, **46**, 4706–4715.
Knapp, J. E., Pahl, R., Srajer, V. & Royer, W. E. Jr (2006). *Proc. Natl Acad. Sci. USA*, **103**, 7649–7654.
Matsen, F. A. & Franklin, J. L. (1950). *J. Am. Chem. Soc.* **72**, 3337–3341.
McRee, D. E. (1999). *Practical Protein Crystallography*, 2nd ed. San Diego: Academic Press.
Moffat, K. (1989). *Annu. Rev. Biophys. Biophys. Chem.* **18**, 309–323.
Moffat, K. (2001). *Chem. Rev.* **101**, 1569–1581.
Peters, G. & Wilkinson, J. H. (1971). *Numer. Math.* **16**, 181–204.
Rajagopal, S., Anderson, S., Srajer, V., Schmidt, M., Pahl, R. & Moffat, K. (2005). *Structure*, **13**, 55–63.
Rajagopal, S., Kostov, K. S. & Moffat, K. (2004). *J. Struct. Biol.* **147**, 211–222.
Rajagopal, S., Schmidt, M., Anderson, S., Ihee, H. & Moffat, K. (2004). *Acta Cryst.* D**60**, 860–871.
Ren, Z., Bourgeois, D., Helliwell, J. R., Moffat, K., Šrajer, V. & Stoddard, B. L. (1999). *J. Synchrotron Rad.* **6**, 891–917.
Ren, Z., Perman, B., Šrajer, V., Teng, T., Pradervand, C., Bourgeois, D., Schotte, F., Ursby, T., Kort, R., Wulff, M. & Moffat, K. (2001). *Biochemistry*, **40**, 13788–13801.
Schlichting, I. (2003). *Biospektrum*, **2**, 153–155.
Schlichting, I., Almo, S. C., Rapp, G., Wilson, K., Petrakos, K., Lentfer, A., Wittinghofer, A., Kabsch, W., Pai, E. F., Petsko, G. A. & Goody, R. S. (1990). *Nature* (*London*), **345**, 309–315.
Schmidt, M. (2008). *Ultrashort Laser Pulses in Medicine and Biology*, edited by W. Zinth, M. Braun & P. Gilch, pp. 201–241. Heidelberg, New York: Springer Verlag.
Schmidt, M., Ihee, H., Pahl, R. & Srajer, V. (2005). *Methods in Molecular Biology*, Vol. 305, *Protein–Ligand Interactions: Methods and Applications*, edited by G. U. Nienhaus, pp. 115–154. Totowa: Humana Press.
Schmidt, M., Nienhaus, K., Pahl, R., Krasselt, A., Nienhaus, U., Parak, F. & Srajer, V. (2005). *Proc. Natl Acad. Sci. USA*, **13**, 11704–11709.
Schmidt, M., Pahl, R., Srajer, V., Anderson, S., Ren, Z., Ihee, H., Rajagopal, S. & Moffat, K. (2004). *Proc. Natl Acad. Sci. USA*, **101**, 4799–4804.
Schmidt, M., Rajagopal, S., Ren, Z. & Moffat, K. (2003). *Biophys. J.* **84**, 2112–2129.
Singeleton, R. C. (1968). *IEEE Trans. Audio Electroacoust.* **AU-17**, 93–102.
Steinfeld, J. I., Francisco, J. S. & Hase, W. L. (1989). *Chemical Kinetics and Dynamics*. Englewood Cliffs: Prentice Hall.